QoS Enhancement in Rural Areas Through Energy-Efficient UAV-Assisted NOMA and OMA Data Transmission Utilizing Wide Elliptical Beam

Tushar Bose, Nilesh Chatur, *Student Member, IEEE*, Mithun Mukherjee, *Senior Member, IEEE* and Aneek Adhya, *Member, IEEE*

***Abstract*—In this work, we present a framework to provide network services to fixed home users in rural areas through joint utilization of fifth-generation (5G) next-generation node B (gNB) and an unmanned aerial vehicle (UAV), wherein, users outside the service area of gNB are served by the UAV. In this regard, we propose an optimization framework to maximize the coverage radius of the gNB considering the 5G rural macro (RMa) propagation scenario. Next, we propose optimization frameworks for UAV-assisted non-orthogonal multiple access (NOMA) and orthogonal multiple access (OMA) data transmission schemes. The aforementioned frameworks for UAV-assisted data transmission schemes minimize the communication power and compute the optimal UAV hovering height to meet the desired QoS requirements of the users. Thereafter, we investigate a framework to design a wide elliptical beam to serve the users under the coverage of the UAV. Next, in this paper, we present an exhaustive mathematical framework to determine the angular velocity of the rotors, the total current consumed by the rotors and the hovering power consumption of the UAV, wherein the UAV hovers at the optimal height depending upon the NOMA or OMA data transmission scheme. We propose a graphical methodology to compute the battery life of the UAV. The simulation results demonstrate that the proposed method of UAV-assisted NOMA and OMA data transmission coupled with the wide elliptical beam significantly reduces the communication power requirements to meet the desired QoS requirements of the ground users as compared to the conventional UAV-assisted NOMA and OMA transmission schemes. Furthermore, the proposed methodology considerably enhances the battery life of the UAV, thereby resulting in a greater hovering time of the UAV compared to the conventional UAV-assisted NOMA and OMA transmission schemes.**

***Index Terms*—Unmanned aerial vehicle (UAV), Wide elliptical beam, UAV-assisted NOMA and OMA, UAV Battery life.**

I. Introduction

The present-day fifth-generation (5G) networks provide high data rates, massive connectivity, and support advanced applications such as augmented reality and virtual reality. However, the digital divide, i.e., the availability of internet and communication technologies (ICT) between rural and urban areas, continues to widen [1], resulting in the risk of deprivation of advanced technologies derived from ICT in rural areas. Compared to urban cities rural areas suffer from poor infrastructure and limited power, making the return on investment (ROI) difficult for telecom operators in rural areas.

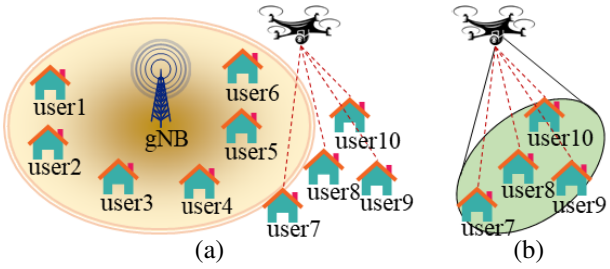

Fig. 1 System model: the spatially separated users over a geographical area of interest have to be provided network services where (a): shows that the users outside the coverage radius of gNB are served by UAV and (b): depicts UAV-assisted NOMA or OMA data transmission through the design of a wide elliptical beam.

Numerous technologies such as satellites, optical fiber links, microwave links, and unmanned aerial vehicles (UAVs) have been investigated to provide network services to rural areas, thereby promoting the reduction of the digital divide. Satellites can provide a direct communication link to rural areas without the need for infrastructure, i.e., without the need for 5G next-generation node B (gNB) and electricity grid. However, satellites incur high deployment costs and relatively high latency compared to other technologies [2]. Transmission through optical fiber is a promising technology for long-distance communication in rural areas. However, challenging terrain and the low population density of rural areas result in high maintenance costs and a low ROI for optical fiber deployment in rural areas. Providing wireless connections through microwave links utilizing gNBs is an effective solution. However, the lack of proper infrastructure for the electric grid and energy storage facilities makes the installation of multiple gNBs challenging in rural environments.

The cost-effectiveness and flexible deployment of UAVs make them a promising solution for providing network services to rural areas. Furthermore, the high payload-carrying capacity of present-day UAVs enables them to carry base stations (BSs) and servers to remote rural locations. Further, fewer buildings and scatterers in rural scenarios enable the UAV to establish direct line of sight (LoS) communication with the users, thereby enhancing the overall quality-of-service (QoS). Moreover, the UAVs can act as an aerial relay to provide network services to users outside the gNB.

Motivated by the aforementioned benefits of UAV to provide

T. Bose, N. Chatur, and A. Adhya are with the G. S. Sanyal School of Telecommunication, IIT Kharagpur, 721302, India (e-mail: btushar@kgpian.iitkgp.ac.in; nileshchatur@iitkgp.ac.in; aneek@gssst.iitkgp.ac.in).

M. Mukherjee is with the Computer and Communication Engineering, Khalifa University, Abu Dhabi, 127788, UAE (email: mithun.mukherjee@ku.ac.ae).

ICT in rural areas, we investigate a joint framework of utilizing a UAV along with a gNB to provide network services to the fixed home users present over a geographical area of interest. Depending on the users' request for network services, a UAV is deployed to serve the users outside the coverage of gNB. In this paper, we investigate both UAV-assisted non-orthogonal access (NOMA) and orthogonal multiple access (OMA) data transmission schemes. Furthermore, we investigate a framework for wide elliptical beam generation to serve the users under the coverage of the UAV. In this work, we also present a detailed study regarding hovering and the communication power requirements of the UAV.

The rest of the paper is organized as follows: Section II discusses related works and our contributions. Section III presents the system model of this work. In Section IV, we discuss the mathematical optimization framework to maximize the coverage radius of gNB. Section V, discusses the channel model for communication between the UAV and ground users. We present the optimization frameworks of UAV-assisted NOMA and OMA data transmission to compute the minimum communication power and optimal UAV height in Section VI. In Section VII we present the framework for designing a wide elliptical beam to serve the users associated with the UAV. In Section VIII, we present a mathematical framework to compute the hovering power and battery life of the battery-powered UAV hovering at an optimal height for NOMA and OMA data transmission schemes. Section IX simulation results and performance evaluation of the proposed framework. Finally, Section X concludes this paper.

II. Related Works and Contributions

In this section, we discuss the related works and our contributions pertaining to UAV-assisted network deployment in rural areas.

A. Related Works on Enhancing ICT in Rural Areas Utilizing UAVs

Authors in [3] utilized a stochastic geometry-based framework for coverage analysis in UAV-assisted cellular networks in rural areas. However, optimization of height and communication power of UAV, and UAV-assisted NOMA and OMA transmission were not widely considered in [3]. Authors in [4] explored path planning for autonomous UAV motion in rural areas experiencing weak communication signal strength. The authors in [5] used the long-term evolution (LTE) network as the infrastructure for UAV communication and data transfer in rural areas. The authors studied the communication characteristics of an LTE-connected UAV at different altitudes and showed that a higher elevation of the UAV benefits from better signal quality and experiences fewer handover processes.

B. Related Works on UAV-Assisted NOMA and OMA Data Transmission

In recent years, various studies have been undertaken for UAV-aided NOMA data transmission. Authors in [6] carried out a stochastic geometry-based performance evaluation of NOMA-aided UAV networks. The authors investigated a joint trajectory design and power allocation for static NOMA users based on a simplified two-dimensional (2D) model of a UAV flying at a fixed height. However, in the framework of [6] optimization for communication power and height of UAV for desired QoS was not widely studied.

Authors in [7] presented a performance evaluation framework for UAV relays utilizing amplify-and-forward and decode-and-forward relaying protocols employing the NOMA technique. In their work, the authors consider the UAV relay to harvest energy from nearby BS and present the closed-form expressions of outage probabilities and ergodic capacities for each UAV relaying protocol. However, the work of [7], considered only two NOMA-assisted users and further the height optimization of the UAV, and communication power minimization were not widely studied. Recently, authors in [8] maximized the UAV-BS energy efficiency for data traffic collection from the gateways under the constraints of total serving delay, UAV-BS flying speed, and transmitting power of gateways. The authors considered NOMA transmission to the UAV-BS and proposed theorems for optimizing the UAV hovering height to minimize the transmitting power of the gateway. However, the rotor velocities, current drawn by the rotors, battery discharge of hovering UAV and wide beam design were not widely studied. Authors in [9], investigated the application of the NOMA technique into the UAV aided relay networks. Specifically, the authors formulated a joint UAV height optimization, channel allocation, and power allocation problem to maximize the total data rate of the cell edge users under the coverage of the UAV. However, the power consumption of hovering UAV, and the battery life of UAV were not widely considered in [9]. In another recent work, [10] the authors maximize the data collection throughput from ground nodes utilizing a NOMA and OMA-assisted rotatory-wing UAV.

From the above analysis, it can be deduced that a joint holistic framework (wherein the spatially separated users in a given area are served via a UAV along with a gNB), incorporating the determination of the optimal coverage radius of gNB, location of gNB, and the optimal location of the UAV to serve the users outside the coverage area of gNB coupled with height optimization and communication power minimization of the UAV for NOMA and OMA transmission schemes to serve multiple users, along with a wide elliptical beam design, has not been widely considered. Further, the battery life of the UAV hovering at an optimal height, depending on NOMA or OMA transmission incorporating the rotor velocities and current drawn by the UAV has not been widely studied.

C. Contributions

The main contributions of this paper are summarized as follows:

- We present an optimization framework to compute the optimal coverage radius of gNB, to serve the fixed home users present in a rural area, by utilizing the 5G third-generation partnership project (3GPP) rural macro (RMa) propagation scenario. For users outside the coverage area of the gNB, we compute the optimal 2D location of the

UAV through an unsupervised machine learning (ML) framework.

- We propose optimization frameworks for UAV-assisted NOMA and OMA data transmission schemes. To promote an energy-efficient UAV deployment, thereby increasing the service time of the battery-powered UAV, the optimization framework minimizes the communication power requirement for NOMA and OMA-assisted data transmission to satisfy the users' desired QoS outside the gNB coverage. Moreover, the optimization frameworks also compute the optimal hovering height of the UAV to meet the QoS requirements. Furthermore, the optimum height of the UAV is computed by taking into account the maximum height of buildings and the flight regulations of the geographical area of interest.
- To compute the optimal power and height of UAV we utilize a realistic air-to-ground (ATG) channel model incorporating LoS probability, non-line of sight (NLoS) probability, LoS and NLoS pathloss (PL), variation of Rician factor with the elevation angle of UAV, and variation of PL exponent with the height of the UAV.
- We propose the design of a wide elliptical beam to serve the users outside the coverage of the gNB present in a given geographical area of interest.
- We present an extensive mathematical framework to compute the angular velocity of rotors, total current consumption, and the hovering power consumption of the UAV, wherein the UAV hovers at an optimal height depending upon the NOMA or OMA transmission. Furthermore, we propose a graphical methodology to compute the battery life of the UAV.
- The proposed methodology of the utilization of a wide elliptical beam along with UAV-assisted NOMA and OMA data transmission yields better performance in terms of communication power requirement and battery life of the UAV as compared to the conventional UAV-assisted NOMA and OMA transmission schemes.

III. System Model

The system model used in this study is shown in Fig. 1. We consider that fixed home users over a geographical area of interest have to be provided with network services. Primarily, the users are provided network services through a gNB, whereas the users outside the coverage radius of gNB are served through a UAV. The UAV hovers at an optimal location, consuming minimum transmit power to meet the users' desired QoS. We consider the ground to be a 2D $x-y$ plane and the hovering height of the UAV is considered to be along the z axis.

The set of all users requesting network services in the geographical area is referred as the user set and denoted by U^a, where $U^a = \left\{u_1^a, u_2^a, \cdots, u_i^a, \cdots, u_{N_a}^a\right\}$. The i^{th} user in the user set is denoted by u_i^a, and N_a is the total number of users in the area. The set of users served by the gNB is represented as the gNB set and denoted by U^g, where $U^g = \left\{u_1^g, u_2^g, \cdots, u_i^g, \cdots, u_{N_g}^g\right\}$. The i^{th} user in gNB set is represented as u_i^g, and the total number of users under the coverage radius of gNB is N_g. The set of users served through the UAV is referred to as the UAV set, and denoted by U^d. Here, $U^d = \left\{u_1^d, u_2^d, \cdots, u_i^d, \cdots, u_{N_d}^d\right\}$, where the i^{th} user in UAV set is u_i^d, and N_d is the number of users served by the UAV. The relations among sets U^a, U^g, and U^d is given as

$$U^g \cup U^d = U^a \tag{1}$$

$$U^g \cap U^d = \emptyset. \tag{2}$$

Equation (1) signifies that all users in the area are served either by the gNB or UAV. Equation (2) indicates that a given user in the geographical area of interest ($u_i^a \in U^a$) is not simultaneously served via both the gNB and UAV.

The x coordinates of user u_i^a, u_i^g, and u_i^d is denoted by u_{ix}^a, u_{ix}^g, and u_{ix}^d respectively. Similarly, the y coordinates of user u_i^a, u_i^g, and u_i^d is denoted by u_{iy}^a, u_{iy}^g, and u_{iy}^d respectively. The location of gNB incorporating the spatial distribution of users in the geographical area is denoted by (x_G, y_G). The x and y coordinates of the optimal 2D projection of the UAV on the ground are denoted by x_D and y_D respectively. The UAV hovers at a height of h_D along the z axis to provide network services to users outside the gNB.

IV. Computation of Optimal Coverage radius of gNB

The optimal radius of the gNB placed at (x_G, y_G) is computed such that the desired QoS characterized by the coverage probability is satisfied within the coverage radius of the gNB. The LoS and NLoS probabilities (P_{los}^{rma} and P_{nlos}^{rma}, respectively) for the RMa propagation scenario are expressed as

$$P_{los}^{rma} = e^{-\frac{(r_g-10)}{1000}} \;\&\; P_{nlos}^{rma} = 1 - P_{los}^{rma} \quad \text{where,} \tag{3}$$

r_g is the radius of the gNB. We consider the operating frequency of gNB as 28 GHz, and utilizing the parameters in [11], we derive the PL for the LoS propagation scenario (PL_{los}^{rma}) as

$$\begin{aligned} PL_{los}^{rma} &= 60.684 + 0.00139\sqrt{1122.25 + r_g^2} + \\ &\quad 4.446 \log_e\left(1122.25 + r_g^2\right). \end{aligned} \tag{4}$$

The PL for NLoS propagation scenario (PL_{nlos}^{rma}) is derived as

$$PL_{nlos}^{rma} = 32.5765 + 8.38 \log_e\left(1122.25 + r_g^2\right). \tag{5}$$

The combined PL (PL^{rma}) incorporating LoS and NLoS probabilities for RMa propagation scenario is expressed as

$$PL^{rma} = P_{los}^{rma} \times PL_{los}^{rma} + P_{nlos}^{rma} \times PL_{nlos}^{rma}. \tag{6}$$

The received signal power (P_r^{rma}) is computed as

$$P_r^{rma} = P_t^{rma} - PL^{rma} - X_\sigma \quad \text{where,} \tag{7}$$

P_t^{rma} is the transmit power of the gNB, and X_σ is the log-normal random variable representing the shadowing phenomena. The coverage probability (P_{cov}^{rma}) is defined as the probability of the received signal power being greater than the threshold P_{min}. Mathematically, P_{cov}^{rma} is expressed as

$$P_{cov}^{rma} = P\left(P_t^{rma} - PL^{rma} - X_\sigma \geq P_{min}\right). \tag{8}$$

The closed-form expression for P_{cov}^{rma} is written as

$$P_{cov}^{rma} = 1 - \frac{1}{2} erfc\left(\frac{P_t^{rma} - PL^{rma} - P_{min}}{\sqrt{2}\sigma}\right) \text{ where, } (9)$$

$erfc$ is the complementary error function and σ is the standard deviation of X_σ. The optimization problem for maximizing the coverage radius of gNB is formulated as

$$R_g^\star = \text{Maximize } r_g \quad (10)$$

$$\text{Subject to:} \quad P_{cov}^{rma} \geq \gamma_{cov}\,, \quad r_g \geq 0. \quad (11)$$

As shown in equation (10), the optimization problem maximizes the coverage radius of gNB $R_g^\star$. Equation (11) ensures that the coverage probability is larger than the coverage probability threshold γ_{cov}. We solve the proposed gNB coverage radius maximization framework by utilizing the constrained Nelder-Mead optimization technique [12]. The coverage area of the gNB is a circle with radius $R_g^\star$ centered at (x_G, y_G). The users inside the coverage area of the gNB constitute the gNB set (i.e., U^g).

V. Channel Model for UAV to Ground Communication

In this section, we present the mathematical framework of the ATG channel for communication from UAV to ground users.

A. ATG Channel

The received signal from the UAV to the ground users consists of a strong LoS and scattered signal components. The channel from UAV to the ground users is modelled suitably by Rician distribution [13]. The ATG channel $\mathfrak{h}_{u_i}^d$ from UAV to user u_i^d is expressed as

$$\mathfrak{h}_{u_i}^d = \frac{\mathfrak{g}_{u_i}^d}{\sqrt{PL_{u_i}^d}} \text{ where, } (12)$$

$\mathfrak{g}_{u_i}^d$ is a random variable corresponding to the small-scale fading effects and $PL_{u_i}^d$ is the large-scale PL between UAV and u_i^d. The channel gain $\left|\mathfrak{g}_{u_i}^d\right|^2$ follows a non-central chi-square distribution with probability density function given as

$$f_{\left|\mathfrak{g}_{u_i}^d\right|^2}(x) = \frac{\left(1+K_{u_i}^d\right)e^{-K_{u_i}^d}}{\Omega} \times e^{-\frac{\left(1+K_{u_i}^d\right)x}{\Omega}} \times I_0\left(2\sqrt{\frac{K_{u_i}^d\left(1+K_{u_i}^d x\right)}{\Omega}}\right) \text{ where, } (13)$$

$$\Omega = \mathbb{E}\left[\left|\mathfrak{g}_{u_i}^d\right|^2\right] = 1\,.$$

$K_{u_i}^d$ is the Rician factor, $\mathbb{E}$ denotes the expectation operator, Ω is the normalized average fading power, and $I_0(.)$ is the zeroth-order modified Bessel function of the first kind. The cumulative distribution function of $\left|\mathfrak{g}_{u_i}^d\right|^2$ is expressed as

$$F_{\left|\mathfrak{g}_{u_i}^d\right|^2}(x) = 1 - Q\left(\sqrt{2K_{u_i}^d}, \sqrt{2\left(1+K_{u_i}^d\right)x}\right) \text{ where, } (14)$$

Q denotes the Marcum Q function of first order and is expressed as

$$Q(y_1, y_2) \overset{\text{def}}{=} \int_{y_2}^{\infty} e^{-\frac{y_1^2+y_2^2}{2}} I_0(y_1 x)\, dx. \quad (15)$$

B. Model of Rician Factor

The Rician factor is defined as the ratio of the power of the LoS component to the power of multipath components and is modeled as a function of the elevation angle [14]. As observed from Fig. 2, the elevation angle of user u_i^d $\left(u_i^d \in U^d\right)$ with respect to UAV can be expressed as

$$\theta_{u_i}^d = \arctan\left(\frac{h_D}{r_{u_i}^d}\right), \theta_{u_i}^d \in \left[0, \frac{\pi}{2}\right] \text{ where,}$$
$$r_{u_i}^d = \sqrt{\left(x_D - u_{ix}^d\right)^2 + \left(y_D - u_{iy}^d\right)^2}. \quad (16)$$

The Rician factor $K_{u_i}^d$ for user u_i^d as a function of elevation

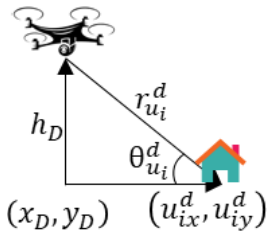

Fig. 2 Elevation angle of a user u_i^d with respect to UAV.

angle is given as [13]

$$K_{u_i}^d = a \times e^{b\theta_{u_i}^d} \text{ where, } (17)$$

a and b are the environment-dependent constants expressed as

$$a = k_0, \text{ and } b = \frac{2}{\pi}\log_e\left(\frac{k_{\frac{\pi}{2}}}{k_0}\right). \quad (18)$$

As observed from equations (16) and (17), each user u_i^d served by UAV experiences a different Rician factor $K_{u_i}^d$. The difference in $K_{u_i}^d$ arises as the LoS condition of users differs with respect to UAV. The difference in the LoS condition arises by virtue of the different spatial locations of the users $\left(u_i^d \in U^d, i = 1, 2, \cdots, N_d\right)$ with respect to UAV.

C. ATG PL Model

The LoS probability of user u_i^d with respect to UAV is modeled by using a sigmoid function and is expressed as [15]

$$P_{los}^{u_i^d} = \frac{1}{1 + Ae^{-B\left(\theta_{u_i}^d - A\right)}} \text{ where, } (19)$$

$P_{los}^{u_i^d}$ denotes the LoS probability of u_i^d with respect to UAV. A and B are constants depending upon the propagation environment. From equation (19), it is observed that $P_{los}^{u_i^d}$ depends on the elevation angle $\theta_{u_i}^d$, which in turn depends on the height h_D of UAV and the spatial location of u_i^d with respect to UAV. The NLoS probability $P_{nlos}^{u_i^d}$ is given as $P_{nlos}^{u_i^d} = 1 - P_{los}^{u_i^d}$. The

PL encountered for communication from UAV to u_i^d for LoS scenario $\left(PL_{los}^{u_i^d}\right)$ is given as [15]

$$PL_{los}^{u_i^d} = 20\alpha_{u_i}^d \log_{10}\left(\sqrt{r_{u_i^d}^2 + h_D^2}\right) + 20\log_{10}(f) + 20\log_{10}\left(\frac{4\pi}{c}\right) + \eta_{los} \text{ where,} \tag{20}$$

f is the operating frequency of UAV, c is the speed of light, and η_{los} is the excessive PL due to LoS propagation. The PL exponent $\left(\alpha_{u_i}^d\right)$ between u_i^d and UAV is typically proportional to the density of obstacles. Therefore, $\alpha_{u_i}^d$ is characterized by utilizing the notion of $P_{los}^{u_i^d}$, and is expressed as [13]

$$\alpha_{u_i}^d = \alpha_1 P_{los}^{u_i^d} + \beta_1 \text{ where,} \tag{21}$$

α_1 and β_1 are constants depending upon the environmental characteristics and the operating frequency. α_1 and β_1 are expressed as $\alpha_1 = \alpha_{\frac{\pi}{2}} - \alpha_0$ and $\beta_1 = \alpha_0$. The PL encountered for communication from UAV to u_i^d for NLoS scenario $\left(PL_{nlos}^{u_i^d}\right)$ is given as

$$PL_{nlos}^{u_i^d} = 20\alpha_{u_i}^d \log_{10}\left(\sqrt{r_{u_i^d}^2 + h_D^2}\right) + 20\log_{10}(f) + 20\log_{10}\left(\frac{4\pi}{c}\right) + \eta_{nlos} \text{ where,} \tag{22}$$

η_{nlos} is the excessive PL due to NLoS propagation condition. PL for communication from UAV to u_i^d incorporating the effects of LoS probability, NLoS probability, PL due to LoS and NLoS is denoted by $PL^{u_i^d}$ and is expressed as

$$PL^{u_i^d} = P_{los}^{u_i^d} \times PL_{los}^{u_i^d} + P_{nlos}^{u_i^d} \times PL_{nlos}^{u_i^d}. \tag{23}$$

Utilizing equation (12), the channel from UAV to u_i^d incorporating the effects of the LoS probability, NLoS Probability, PL due to LoS and NLoS, and small scale fading is written as

$$\mathfrak{h}_{u_i}^d = \frac{\mathfrak{g}_{u_i}^d}{\sqrt{P_{los}^{u_i^d} \times PL_{los}^{u_i^d} + P_{nlos}^{u_i^d} \times PL_{nlos}^{u_i^d}}}. \tag{24}$$

VI. UAV-Assisted NOMA and OMA Data Transmission

This section presents the mathematical frameworks for communication power minimization and height optimization of UAV-assisted NOMA and OMA data transmission.

A. UAV-Assisted NOMA Transmission

The users outside the coverage radius of gNB $R_g^\star$ are served by the UAV placed at (x_D, y_D). For NOMA transmission, the UAV serves all users in the UAV set U^d simultaneously via power domain NOMA, utilizing the entire system bandwidth [16]. To deploy NOMA, the channels of the users in U^d are sorted in the order: $\left|\mathfrak{h}_{u_1}^d\right|^2 \leq \left|\mathfrak{h}_{u_2}^d\right|^2 \leq \cdots \left|\mathfrak{h}_{u_i}^d\right|^2 \leq \cdots \leq \left|\mathfrak{h}_{u_{N_d}}^d\right|^2$. UAV transmits the superimposed information signal $\mathrm{x}^d = \sum_{i=1}^{N_d} \sqrt{a_{u_i}^d P_d}\mathrm{x}_{u_i}^d$, where P_d is the power transmitted by UAV, $a_{u_i}^d$ is the fraction of P_d transmitted to u_i^d, and $\mathrm{x}_{u_i}^d$ is the signal for u_i^d. User u_i^d receives signal $\mathrm{y}_{u_i}^d$ given by

$$\mathrm{y}_{u_i}^d = \mathfrak{h}_{u_i}^d \sum_{i=1}^{N_d} \sqrt{a_{u_i}^d P_d} \times \mathrm{x}_{u_i}^d + w_{u_i}^d \text{ where,} \tag{25}$$

$w_{u_i}^d$ is the additive white Guassian noise at u_i^d with zero mean and variance σ_n^2. The power allocation factor $a_{u_i}^d$ as

$$a_{u_i}^d = \frac{r_{u_i}^d}{\sum_{i=1}^{N_d} r_{u_i}^d}. \tag{26}$$

After receiving the signal $\mathrm{y}_{u_i}^d$, each user u_i^d performs SIC. User u_i^d decodes the signals from the weaker users, i.e., each user u_i^d decodes the signal for each u_m^d, where $m < i$. To decode the signal of user u_i^d, the signals from the weaker users are subtracted from the received signal $\mathrm{y}_{u_i}^d$, treating the signals from the stronger users $u_m^d, m > i$ as interference. Therefore, following the principle of SIC, the achievable rate of user $u_i^d, i < N_d$ denoted by $\mathcal{R}_{noma}^{u_i^d}$ is expressed as

$$\mathcal{R}_{noma}^{u_i^d} = \log_2\left(1 + \frac{P_d \times a_{u_i}^d \left|\mathfrak{h}_{u_i}^d\right|^2}{P_d \left|\mathfrak{h}_{u_i}^d\right|^2 \sum_{m=i+1}^{N_d^d} a_{u_m}^d + \sigma_n^2}\right). \tag{27}$$

The achievable rate of user $u_{N_d}^d$ denoted by $\mathcal{R}_{noma}^{u_{N_d}^d}$ is expressed as

$$\mathcal{R}_{noma}^{u_{N_d}^d} = \log_2\left(1 + \frac{P_d \times a_{u_{N_d}}^d \left|\mathfrak{h}_{u_{N_d}}^d\right|^2}{\sigma_n^2}\right). \tag{28}$$

The outage probability of user u_i^d is denoted by $\mathcal{P}_{noma}^{u_i^d}$ and is derived as

$$\mathcal{P}_{noma}^{u_i^d} = 1 - Q\left(\sqrt{2K_{u_i}^d}, \sqrt{\frac{2\left(1+K_{u_i}^d\right)\phi_{u_i}^d PL^{u_i^d}\sigma_n^2}{P_d\left(a_{u_i}^d - \phi_{u_i}^d\left(\sum_{m=i+1}^{N_d^d} a_{u_m}^d\right)\right)}}\right), \quad \phi_{u_i}^d = 2^{\mathcal{R}_t^{u_i^d}} - 1 \quad \& \quad i \neq N_d \quad \text{where,} \tag{29}$$

$\mathcal{R}_t^{u_i^d}$ is the target rate (or the desired rate) of u_i^d served by the UAV. The outage probability of user $u_{N_d}^d$ utilizing NOMA transmission, is denoted by $\mathcal{P}_{noma}^{u_{N_d}^d}$ and is derived as

$$\mathcal{P}_{noma}^{u_{N_d}^d} = 1 - Q\left(\sqrt{2K_{u_{N_d}}^d}, \sqrt{\frac{2\left(1+K_{u_{N_d}}^d\right)\phi_{u_{N_d}}^d PL^{u_{N_d}^d}\sigma_n^2}{P_d \times a_{u_{N_d}}^d}}\right)$$

$$\phi_{u_{N_d}}^d = 2^{\mathcal{R}_t^{u_{N_d}^d}} - 1 \quad \text{where,} \tag{30}$$

$\mathcal{R}_t^{u_{N_d}^d}$ is the target rate (or the desired rate) of user N_d served by UAV.

From equations (29) and (30), it may be observed that the outage probability is a function of the transmit power and the height of UAV (as Rician factor, LoS probability,

NLoS probability, and PL are functions of UAV height). We formulate the optimization problem for transmit power minimization for UAV-assisted NOMA transmission as

$$P^{\star}_{d,noma},\, h^{\star}_{D,noma} = \text{Minimize}\;\; P_d \tag{31}$$

$$\text{Subject to:}\quad \mathcal{P}^{u^d_i}_{noma} \leq \epsilon_{th}\; \forall u^d_i \in U^d \tag{32}$$

$$h_{min} \leq h_D \leq h_{max} \tag{33}$$

$$P_d \geq 0 \tag{34}$$

The objective function (31) minimizes the communication power requirement of UAV under the NOMA transmission scheme. The output of the optimization problem is the optimal communication power $P^{\star}_{d,noma}$ and the optimal UAV height $h^{\star}_{D,noma}$. Constraint (32) ensures that the outage probability of all users served by UAV should be less than or equal to the threshold ϵ_{th}, thereby ensuring the QoS characterized by outage probability. Constraint (33) ensures that the hovering height of UAV is between h_{min} and h_{max}, where h_{min} denotes the maximum height of the buildings in the area of interest and h_{max} the maximum permissible height of the UAV governed by the flight regulations in the geographical area. Constraint (34) puts the lower bound for the communication power requirement. We utilize the differential evolution algorithm [17] to solve the proposed optimization problem of UAV-assisted NOMA transmission.

B. UAV-Assisted OMA Transmission

The rate of user u^d_i utilizing UAV-assisted OMA transmission is denoted by $\mathcal{R}^{u^d_i}_{oma}$ and is expressed as

$$\mathcal{R}^{u^d_i}_{oma} = \frac{1}{N_d}\log_2\left(1+\frac{P_d \times \left|\mathfrak{h}^d_{u_i}\right|^2}{\sigma^2_n}\right). \tag{35}$$

The outage probability of u^d_i utilizing OMA-assisted transmission is denoted by $\mathcal{P}^{u^d_i}_{oma}$ and is expressed as

$$\mathcal{P}^{u^d_i}_{oma} = 1 - Q\left(\sqrt{2K^d_{u_i}}, \sqrt{\frac{2\left(1+K^d_{u_i}\right)\phi^d_{u_i} P L^{u^d_i}\sigma^2_n}{P_d}}\right)$$

$$\phi^d_{u_i} = 2^{\mathcal{R}^{u^d_i}_t} - 1. \tag{36}$$

The optimization problem for communication power minimization for UAV-assisted OMA data transmission is formulated as

$$P^{\star}_{d,oma},\, h^{\star}_{D,oma} = Minimize\;\; P_d \tag{37}$$

$$\text{Subject to:}\quad \mathcal{P}^{u^d_i}_{oma} \leq \epsilon_{th}\; \forall u^d_i \in U^d \tag{38}$$

$$h_{min} \leq h_D \leq h_{max} \tag{39}$$

$$P_d \geq 0 \tag{40}$$

The objective function (37) minimizes the communication power requirement of the UAV for the OMA transmission. The output of the optimization problem for OMA-assisted transmission is the optimal communication power $P^{\star}_{d,oma}$ and the optimal UAV height $h^{\star}_{D,oma}$. Constraint (38) ensures that the outage probability of all the users served by UAV should be less than or equal to the threshold ϵ_{th}. Constraint (39) ensures that the hovering height of UAV is between h_{min} and h_{max}. Constraint (40) puts a lower bound on the communication power requirement for D to serve users utilizing the OMA transmission. Similar to the UAV-assisted NOMA transmission we utilize the differential evolution methodology to solve the proposed optimization formulation for UAV-assisted OMA transmission.

VII. Coverage of Users through Wide Elliptical Beam

This section presents the mathematical framework for covering the users through a wide elliptical beam. We first present the methodology to compute the minimum area ellipse enclosing the convex polygon formed by the users served by UAV. Next, utilizing the parameters of the minimum area ellipse we present the mathematical framework for designing a wide elliptical beam to serve the users on the ground plane.

A. Computation of Minimum Area Ellipse

The convex hull of the UAV set U^d is the smallest convex set in $\mathbb{R}^2$ (set of real numbers in 2D x-y plane) containing the users $u^d_1, u^d_2, \cdots u^d_i, \cdots u^d_{N_d}$. The convex hull of set U^d is denoted by $\mathcal{H}^d$. As shown in Fig. 3 $\mathcal{H}^d$ is a convex polygon whose vertices are from U^d and contains all the elements of U^d. The vertices of $\mathcal{H}^d$ are denoted by (x_i, y_i), where $i = 1, 2, \cdots, N_p$. The boundary of $\mathcal{H}^d$ consists of N_p straight line segments. The area A_p of the convex polygon $\mathcal{H}^d$ is given as

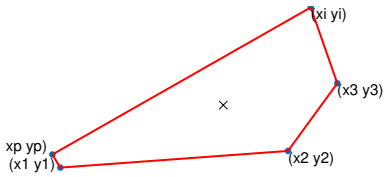

Fig. 3 Pictorial depiction of the convex hull $\mathcal{H}_d$.

$$A_p = \frac{1}{2}\left(\sum_{i=1}^{N_p-1}\left(x_i y_{i+1} - x_{i+1}y_i\right) + x_{N_p}y_1 - x_1 y_{N_p}\right). \tag{41}$$

The x coordinate of the centre of gravity (x_{cg}) of $\mathcal{H}^d$ is expressed as

$$x_{cg} = \frac{1}{6A_p}\left[\sum_{i=1}^{N_p-1}\left(x_i + x_{i+1}\right)\left(x_i y_{i+1} - x_{i+1}y_i\right) + \left(x_{N_p} + x_1\right)\left(x_{N_p}y_1 - x_1 y_{N_p}\right)\right]. \tag{42}$$

Similarly, the y coordinate of the centre of gravity (y_{cg}) of $\mathcal{H}^d$is expressed as

$$y_{cg} = \frac{1}{6A_p}\left[\sum_{i=1}^{N_p-1}\left(y_i + y_{i+1}\right)\left(x_i y_{i+1} - x_{i+1}y_i\right) + \left(y_{N_p} + y_1\right)\left(x_{N_p}y_1 - x_1 y_{N_p}\right)\right]. \tag{43}$$

To compute the minimum area ellipse enclosing $\mathcal{H}^d$, we utilize the method of moments [18]. In this regard, we derive the closed-form expressions for the relevant first and second-order moments of $\mathcal{H}^d$.The first-order moments m_{10} and m_{01} are expressed as $x_{cg} \times A_p$ and $y_{cg} \times A_p$ respectively, whereas the moment m_{11} is given by

$$\begin{aligned} m_{11} = &\sum_{i=1}^{N_p-1} \frac{1}{24}\left(y_{i+1}-y_i\right)\left[\left(y_i+y_{i+1}\right)2x_ix_{i+1}+\right. \\ &\left.\left(3y_i+y_{i+1}\right)x_i^2+\left(y_i+3y_{i+1}\right)x_{i+1}^2\right]+ \\ &\frac{1}{24}\left(y_1-y_{N_p}\right)\left[\left(y_{N_p}+y_1\right)2x_{N_p}x_1+\right. \\ &\left.\left(3y_{N_p}+y_1\right)x_{N_p}^2+\left(y_{N_p}+3y_1\right)x_1^2\right]. \end{aligned} \tag{44}$$

The second order moments m_{20} and m_{02} are expressed as

$$\begin{aligned} m_{20} = &\sum_{i=1}^{N_p-1} \frac{1}{12}\left(\frac{\left(x_{i+1}^4-x_i^4\right)\left(y_{i+1}-y_i\right)}{x_{i+1}-x_i}\right)+ \\ &\frac{1}{12}\left(\frac{\left(x_1^4-x_{N_p}^4\right)\left(y_1-y_{N_p}\right)}{x_1-x_{N_p}}\right) \end{aligned} \tag{45}$$

$$\begin{aligned} m_{02} = &\sum_{i=1}^{N_p-1} \frac{1}{12}\left(y_{i+1}-y_i\right)\left[\left(3x_i+x_{i+1}\right)y_i^2+\right. \\ &\left.2y_iy_{i+1}\left(x_i+x_{i+1}\right)+\left(x_i+3x_{i+1}\right)y_{i+1}^2\right]+ \\ &\frac{1}{12}\left(y_1-y_{N_p}\right)\left[\left(3x_{N_p}+x_1\right)y_{N_p}^2+\right. \\ &\left.2y_{N_p}y_1\left(x_{N_p}+x_1\right)+\left(x_{N_p}+3x_1\right)y_1^2\right]. \end{aligned} \tag{46}$$

Utilizing the first and second-order moments the parameters of the minimum area ellipse enclosing $\mathcal{H}^d$ is given as

$$\begin{aligned} a_e &= \left(\frac{m_{20}+m_{02}+\sqrt{\left(m_{20}-m_{02}\right)^2+4m_{11}^2}}{\frac{A_p}{2}}\right)^{\frac{1}{2}} \\ b_e &= \left(\frac{m_{20}+m_{02}-\sqrt{\left(m_{20}-m_{02}\right)^2+4m_{11}^2}}{\frac{A_p}{2}}\right)^{\frac{1}{2}} \\ \phi_e &= \frac{1}{2}\arctan\left(\frac{2m_{11}}{m_{20}-m_{02}}\right) \text{ where,} \end{aligned} \tag{47}$$

a_e, b_e, and ϕ_e denote the semimajor axis, semiminor axis, and tilt angle of the ellipse, respectively. Utilizing the aforementioned parameters, the parametric equation of the minimum area ellipse in x-y plane enclosing $\mathcal{H}^d$ is expressed as

$$\begin{aligned} x &= x_{cg}+a_e\cos\left(\theta_e\right)\cos\left(\phi_e\right)-b_e\sin\left(\theta_e\right)\sin\left(\phi_e\right) \\ y &= y_{cg}+a_e\cos\left(\theta_e\right)\sin\left(\phi_e\right)+b_e\sin\left(\theta_e\right)\cos\left(\phi_e\right), \\ &\text{where, } \theta_e \in [0,2\pi]. \end{aligned} \tag{48}$$

B. Wide Elliptical Beam Design

The wide elliptical beam is designed such that the gain of the beam is maximum at the center of gravity (x_{cg}, y_{cg}) of $\mathcal{H}^d$. The beamwidth (w) of the elliptical beam is given as given as [19]

$$\begin{aligned} &w = w_0\sqrt{1+\left(\frac{h_d^\star}{z_0}\right)^2} \text{ where, } w_0 = \sqrt{\frac{2}{a_e^{-2}+b_e^{-2}}}, \\ &z_0 = \frac{kw_0^2}{2}, \text{ and } k = \frac{2\pi}{\lambda_d} \quad \text{here,} \end{aligned} \tag{49}$$

$h_d^\star$ is the optimal hovering height of UAV depending on the NOMA or OMA transmission and λ_d is the operating wavelength of UAV. The wavefront curvature radius (R) and the Gouy phase (ζ) of the elliptical beam is expressed as [19]

$$R = h_d^\star\left(1+\left(\frac{z_0}{h_d^\star}\right)^2\right) \,\&\, \zeta = \arctan\left(\frac{h_d^\star}{z_0}\right). \tag{50}$$

As the elliptical beam is designed to obtain maximum gain at point (x_{cg}, y_{cg}) at the ground, therefore with respect to UAV the beam gain is maximum at the point $\left(x_{cg}^d, y_{cg}^d\right)$ where $x_{cg}^d = x_{cg} - x_D$ and $y_{cg}^d = y_{cg} - y_D$. To obtain the maximum beam gain at point $\left(x_{cg}^d, y_{cg}^d\right)$ the coordinates of the beam center $\left(x_0^b, y_0^b\right)$ in the source plane (i.e, at the UAV) is given as

$$\begin{bmatrix} x_0^b \\ y_0^b \end{bmatrix} = \begin{bmatrix} \cos\left(\zeta\right) & \sin\left(\zeta\right) \\ -\sin\left(\zeta\right) & \cos\left(\zeta\right) \end{bmatrix} \begin{bmatrix} x_{cg}^d \\ y_{cg}^d \end{bmatrix}. \tag{51}$$

The electric field at the source plane E_0 as a function of x, y is given as

$$\begin{aligned} &E_0\left(x,y\right) = A_0e^{-\left[\left(\frac{x}{\cos(\alpha)a_e}\right)^2+\left(\frac{y}{\cos(\alpha)b_e}\right)^2\right]}\times \\ &e^{-\left[\left(\frac{\left(x-x_0^b\right)\cos(\phi_e)+\left(y-y_0^b\right)\sin(\phi_e)}{a_e}\right)^2+\left(\frac{\left(y-y_0^b\right)\cos(\phi_e)-\left(x-x_0^b\right)\sin(\phi_e)}{b_e}\right)^2\right]} \end{aligned} \tag{52}$$

Here, A_0 is the amplitude of the electric field. The electric field E as a function of x, y at the destination plane (i.e, at the ground) is given as

$$\begin{aligned} &E\left(x,y\right) = A_0e^{-\imath kh_d^\star}\left[\frac{w_0}{w}e^{-\left(\frac{x^2+y^2}{w^2}\right)}+\frac{\imath k}{2R}\left(x^2+y^2\right)-\imath\zeta-\right. \\ &\left.\frac{x_0^b+y_0^b}{w_0^2}+\frac{2}{qw_0^2}\left(x+\imath y\right)\left(x_0^b-\imath y_0^b\right)\right] \text{ where,} \\ &q = 1+\imath\frac{h_d^\star}{z_0} \,\&\, \imath = \sqrt{-1}. \end{aligned} \tag{53}$$

The gain at a point (x, y) on the ground is given by

$$G\left(x,y\right) \approx \left|E\left(x,y\right)\right|^2 \text{ where,} \tag{54}$$

$|.|$ denotes the magnitude. The beamforming gain observed at user u_i^d is obtained by substituting $x = u_{ix}^d - x_D$ and $y = u_{iy}^d - y_D$ in equation (54).

VIII. Computation of Hovering Power of UAV

In this section, we discuss the framework for computing the angular velocity of the UAV rotors, the total current consumption by the rotors, the power requirement of the UAV and the battery life of the UAV hovering at an optimal height depending on the NOMA or OMA transmission.

A. Dynamic model of a Quadrotor UAV

The quadrotor UAV has four rotors and by adjusting the speeds of the rotors the UAV can hover at a desired height. The steady-state thrust (i.e., the UAV has no horizontal or vertical motion) generated by the rotor of a hovering UAV is modelled by momentum theory and is expressed as [20]

$$T_{r_i} = C_t \rho A_{r_i} R_{r_i}^2 \omega_{r_i}^2 \,, \quad A_{r_i} = \pi R_{r_i}^2 \text{ here,} \tag{55}$$

T_{r_i} is the thrust generated by rotor r_i, $i = \{1, 2, 3, 4\}$, and ω_{r_i} are the radius and angular velocity, respectively, of the rotor r_i. Further, C_t denotes the thrust coefficient depending on rotor geometry and ρ denotes the density of air. The density of air as a function of height is given as [21]

$$\rho = \rho_0 e^{-u_0 h_d^\star} \,, \quad u_0 = 9.7 \times 10^{-5} \text{where,} \tag{56}$$

ρ_0 is the average density of air. The relation between the pitch angle (θ_0) of rotor blades and thrust coefficient C_t is expressed as [22]

$$\theta_0 = \frac{6C_t}{\sigma_r C_{l_\alpha}} + \frac{3}{2}\sqrt{\frac{C_t}{2}} \,, \;\; \sigma_r = \frac{N_b c_l}{\pi R_{r_i}} \text{ here,} \tag{57}$$

σ_r denotes the rotor solidity, N_b is the number of blades, c_l is the chord length and C_{l_α} is the 2D lift curve slope of the airfoil section(s). Using equation (57) we derive the closed-form expression of C_t as

$$C_t = \frac{6c_l^2 C_{l_\alpha}^2 N_b^2 + 64 c_l C_{l_\alpha} N_b \pi R_{r_i} \theta_0}{384\pi^2 R_{r_i}^2} - \left(\frac{1}{128\sqrt{3}\pi^2}\right) \times \sqrt{12 c_l^4 C_{l_\alpha}^4 N_b^2 + 256 c_l^3 C_{l_\alpha}^3 N_b^3 \pi R_{r_i} \theta_0}. \tag{58}$$

The reaction torque (Q_{r_i}) due to rotor drag acting on the airframe generated by hovering rotor is expressed as [20]

$$Q_{r_i} = \rho C_q A_{r_i} R_{r_i}^3 \omega_{r_i}^2 \,\&\, C_q = \frac{C_t^{\frac{3}{2}}}{\sqrt{2}} + \frac{1}{8}\frac{N_b c_l}{\pi R_{r_i}} C_{d_0} \text{ here,} \tag{59}$$

C_q is the drag coefficient and C_{d_0} is the zero-lift drag coefficient. Specifically, for a quadrotor UAV wherein $R_{r_i} = R_r$, $\forall i = 1, 2, 3, 4$ the total thrust and torques leading to roll, pitch, and yaw movements of the quadrotor UAV are related to the rotors' speed ω_{r_i} by the following equation:

$$\begin{bmatrix} T_\sum \\ \tau_1 \\ \tau_2 \\ \tau_3 \end{bmatrix} = \underbrace{\begin{bmatrix} \widetilde{C_t} & \widetilde{C_t} & \widetilde{C_t} & \widetilde{C_t} \\ 0 & -\widetilde{C_t} d & 0 & \widetilde{C_t} d \\ -\widetilde{C_t} d & 0 & \widetilde{C_t} d & 0 \\ -\widetilde{C_q} & \widetilde{C_q} & -\widetilde{C_q} & \widetilde{C_q} \end{bmatrix}}_{\Gamma} \begin{bmatrix} \omega_{r_1}^2 \\ \omega_{r_2}^2 \\ \omega_{r_3}^2 \\ \omega_{r_4}^2 \end{bmatrix} \quad \text{where,}$$

$$\widetilde{C_t} = C_t \rho_0 e^{-u_0 h_d^\star} \pi R_r^4 \,\&\, \widetilde{C_q} = C_q \rho_0 e^{-u_0 h_d^\star} \pi R_r^5 \text{ here,} \tag{60}$$

$T_\sum$ is the total thrust generated by the rotors, and τ_1, τ_2, and τ_3 are the torques for roll, pitch, and yaw movements of the UAV. Further, d is the distance of each rotor from the center of the UAV. For a steady-state UAV hovering at a given height, the angular velocity of the rotors ω_{r_i} is obtained by inverting Γ such that $T_\sum = M_d g$, where M_d is the mass of the UAV and g is the acceleration due to gravity, and $\tau_1 = \tau_2 = \tau_3 = 0$. For a quadrotor UAV with $R_{r_i} = R_r, \forall i = 1, 2, 3, 4$, hovering at an optimal height $h_d^\star$ (depending upon NOMA or OMA data transmission), we derive the angular velocity ω_h of the rotors as

$$\omega_h = \frac{\sqrt{\frac{e^{h_d^\star u_0} g M_d}{C_t \rho_0 R_r^4}}}{2\sqrt{\pi}} \,, \; \omega_{r_1} = \omega_{r_2} = \omega_{r_3} = \omega_{r_4} = \omega_h. \tag{61}$$

From equation (61), it is observed that the hovering velocity of the rotors depends on the hovering height of the UAV, the mass of the UAV, air density, the radius of the rotors and the thrust coefficient.

B. Hovering Power Consumption and Battery Life of UAV

The voltage and current drawn by the rotor r_i of UAV hovering at the optimal height $h_d^\star$ (depending on NOMA or OMA data transmission) with an angular velocity of the rotors w_h are given as [23]

$$v_{r_i} = \mathcal{R} i_{r_i} + k_e \omega_h \,\&\, i_{r_i} = \frac{1}{k_t}\left(T_f + k_0 \omega_h^2 + D_f \omega_h\right). \tag{62}$$

Here v_{r_i} and i_{r_i} denote the voltage and current drawn by the rotor r_i respectively; $\mathcal{R}$ denotes resistance. k_e, k_t, T_f, k_0, and D_f denote the motor's voltage constant, torque constant, motor friction torque, drag coefficient, and motor viscous damping coefficient. The hovering power $\left(P_{hov}^d\right)$ and the total power $\left(P_{to}^d\right)$ consumed by the UAV is written as

$$P_{hov}^d = \sum_{i=1}^{4} v_{r_i} i_{r_i} \,\&\, P_{to}^d = P_{hov}^d + P_d^\star \text{ here,} \tag{63}$$

$P_d^\star$ is the optimal communication power required depending upon the NOMA or OMA transmission.

Lithium polymer (LiPo) batteries have been widely utilized to power UAVs, therefore, we consider that the total power requirements P_{to}^d of the UAV are met by LiPo batteries. The discharge of these types of batteries is suitably modelled by utilizing the kinetic battery (KiBa) model [24]. In the KiBa model, the battery charge is divided into two wells: the available charge well (y_1) and the bound charge well (y_2). The differential equations governing the change of charge in the wells for a constant current discharge of $\mathcal{I}_d$ are given as

$$\frac{\mathrm{d}y_1(t)}{\mathrm{d}t} = -\mathcal{I}_\mathrm{d} + k_f\left(\frac{y_2(t)}{1-\mu} - \frac{y_1(t)}{\mu}\right) \,, \; \mu \in \left[0, \quad 1\right] \tag{64}$$

$$\frac{\mathrm{d}y_2(t)}{\mathrm{d}t} = -k_f\left(\frac{y_2(t)}{1-\mu} - \frac{y_1(t)}{\mu}\right), \tag{65}$$

$$y_1(0) = \mu C_{batt} \,, \, y_2(0) = (1-\mu) C_{batt} \text{ and,} \tag{66}$$

$$\mathcal{I}_d = \sum_{i=1}^{4} i_{r_i} + \frac{P_d^\star}{v_{tr}} \text{ here,} \tag{67}$$

t denotes time, and k_f is a parameter limiting the rate of flow of charge between the two wells, and μ is the splitting factor. C_{batt} is the battery capacity, and v_{tr} is the UAV's transceiver

voltage. We solve the coupled differential equations and derive the closed-form expression of y_1 and y_2 as

$$y_1(t) = \frac{\mu\left(C_{batt}(\mu-1) - \mathcal{I}_d t(\mu-1)\right)}{\mu-1} - e^{\frac{-k_f t}{\mu-\mu^2}} \left[\frac{\left((\mu-1)\left(\mathcal{I}_d\mu - \mathcal{I}_d\mu^2\right)\right)}{k_f} + \frac{\mathcal{I}_d\mu e^{\frac{\mu t}{\mu-\mu^2}}(\mu-1)^2}{k_f}\right] \quad (68)$$

$$y_2(t) = e^{\frac{-k_f t}{\mu-\mu^2}}\left[\frac{(\mu-1)\left(\mathcal{I}_d\mu - \mathcal{I}_d\mu^2\right)}{k_f} + \frac{\mathcal{I}_d\mu e^{\frac{k_f t}{\mu-\mu^2}}}{k_f}(\mu-1)^2\right] - C_{batt}(\mu-1) + \mathcal{I}_d t(\mu-1). \quad (69)$$

The battery is considered to be completely discharged when there is no charge left in the available charge well (i.e., $y_1(t) = 0$). In this paper, we propose a graphical methodology to compute the battery lifetime of the UAV (i.e., time t at which $y_1(t) = 0$) hovering at an optimal height to meet the desired QoS depending upon NOMA or OMA-aided transmission.

IX. Simulation Results and Discussions

A. Numerical Analysis of Optimal gNB Coverage Radius and Optimal Location of UAV

Network Scenario: A rural scenario, wherein, 24 users are distributed uniformly over a $200 \times 200\,\mathrm{m}^2$ rectangular area is considered. Similar to the works of [25] and [26], we consider the ground users at random positions. The density of users per square kilometer is along the lines of [27]. The optimal location of gNB (x_G, y_G) incorporating the spatial distribution of users in A is computed by *utilizing the k-means algorithm of the unsupervised ML framework* [28].

Optimal coverage radius of gNB: The simulation parameters utilized to compute the optimal coverage radius of gNB are listed in Table I. The graphs of LoS probability (P_{los}^{rma}) and NLoS probability (P_{nlos}^{rma}) are illustrated in Fig. 4(a). From Fig. 4(a) it is observed that as the distance from gNB or coverage radius of gNB (i.e., r_g) increases, the LoS probability decreases and the NLoS probability increases. Fig. 4(b) illustrates the PL for the LoS condition (PL_{los}^{rma}), the NLoS condition (PL_{nlos}^{rma}), and the combined PL (PL^{rma}) incorporating the effects of the LoS and NLoS conditions. From Fig. 4(b), it is observed that the PL is minimum for the propagation scenarios where LoS dominates, whereas the PL is maximum for dominant NLoS scenarios. Fig. 4(c) illustrates the variation of coverage probability (P_{cov}^{rma}) with r_g, as observed from Fig. 4(c), P_{cov}^{rma} decreases with the increase in r_g. To compute the maximum coverage radius of gNB utilizing the constrained Nelder-Mead optimization technique, we consider the values of contract ratio, expand ratio, reflect ratio, shrink ratio, and tolerance for constraint violations as 0.5, 2, 1, 0.5, and 0.001 respectively. For $\gamma_{cov} = 0.96$, the optimal coverage radius of gNB i.e., $R_g^\star$ is obtained as 109.097 m.

TABLE I: Simulation Parameters for Computation of Optimal gNB Radius

Parameters	Values
Transmitted power by gNB (P_t^{rma})	43 dBm
Received signal strength threshold (P_{min})	-75 dBm
Standard deviation of shadowing (σ)	8 dB
Coverage probability threshold (γ_{cov})	0.96

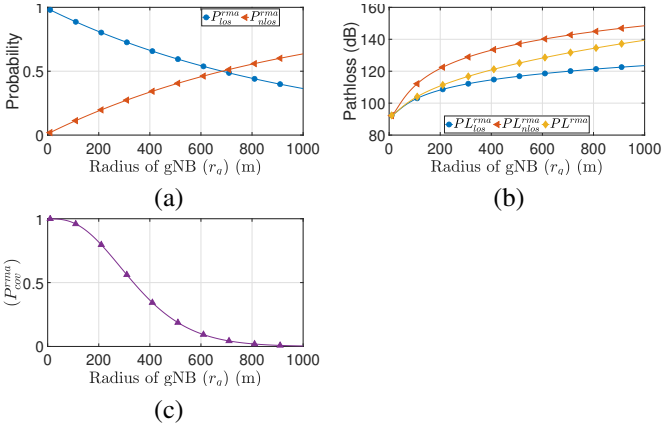

Fig. 4 Variation with respect to coverage radius of gNB (r_g) (a): LoS probability P_{los}^{rma} and NLoS probability P_{nlos}^{rma},(b): PL for LoS condition, NLoS condition and combined PL PL^{rma}, (c): coverage probability P_{cov}^{rma}.

The network deployment, considering the optimal location of gNB, the optimal coverage radius of gNB and the optimal 2D location of the UAV is presented in Fig. 5. As observed from Fig. 5, all the users in the geographical area of interest are not served by the gNB. For the simulated network scenario, 5 users lie outside the coverage of gNB, thereby resulting in the need for UAV-assisted data transmission to provide network services to all the users over the geographical area of interest. The users outside the effective service area of gNB are served by the UAV. The optimal 2D location of the UAV is obtained by utilizing the location information of the users outside the gNB through the k-means algorithm.

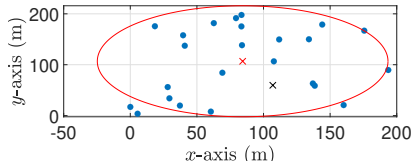

Fig. 5 Network deployment considering optimal coverage radius of the gNB, optimal location of gNB and optimal 2D location of the UAV. The blue dots represent the users over the geographical area of interest. The red cross represents the optimal gNB location, the red circle represents the optimal coverage radius of gNB, and the black cross represents the optimal location of UAV.

B. Numerical Analysis of ATG channel and UAV-Assisted NOMA and OMA data transmission

ATG channel: The parameters used for the simulation of the ATG channel are listed in Table II. As observed from Fig.

TABLE II: Simulation Parameters for ATG Channel

Parameters	Values
Operating frequency of UAV (f)	2 GHz
Speed of light (c)	$3 \times 10^8 \mathrm{ms}^{-1}$
Constants k_0 and $k_{\frac{\pi}{2}}$	3 dB and 15 dB
Constants A and B	11.95 and 0.136
Excessive PL due to LoS propagation (η_{los})	0.1 dB
Excessive PL due to NLoS propagation (η_{nlos})	21 dB
Constants α_0 and $\alpha_{\frac{\pi}{2}}$	3.5 and 2

5, 5 users are served by the UAV. The distances of these 5 users from the UAV are arranged in descending order such that $r^d_{u_1} > r^d_{u_2} > r^d_{u_3} > r^d_{u_4} > r^d_{u_5}$ i.e., the user farthest from the UAV is labelled as user 1 and the nearest user from the UAV is labelled as user 5. The variation of the Rician factor of the users $\left(K^d_{u_i}\right)$ as a function of UAV height (h_D) is illustrated in Fig. 6. As observed from Fig. 6, $K^d_{u_i}$ increases with the

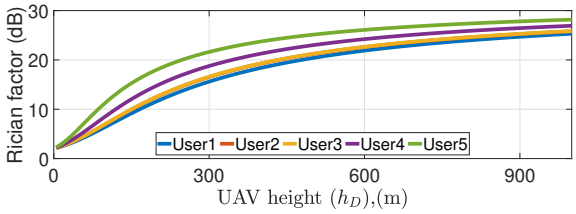

Fig. 6 Ricain factor $\left(K^d_{u_i}\right)$ of users with respect to UAV height h_D.

increase in h_D. This increasing trend of $K^d_{u_i}$, is observed as, with an increase in h_D, the LoS probability increases, thereby resulting in increased signal power through the LoS component. Further, as observed from Fig. 6 various users served by the UAV experience different Rician factors, owing to the different spatial locations of the users with respect to UAV. The LoS probability $P^{u^d_i}_{los}$ of the users served by the UAV as a function of UAV height (h_D) are illustrated in Fig. 7(a). Fig. 7(b) illustrates the NLOS probability $P^{u^d_i}_{nlos}$

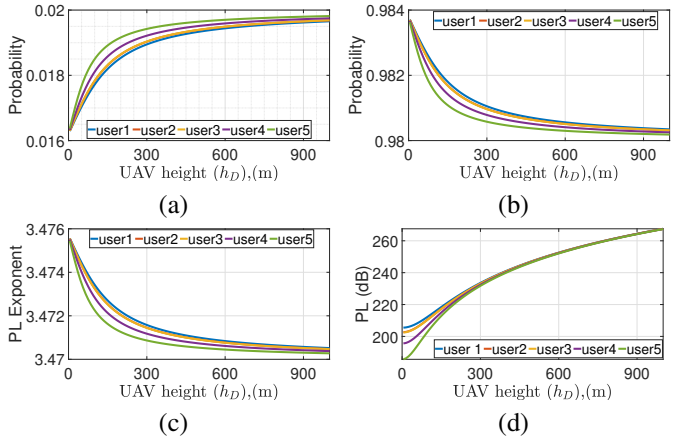

Fig. 7 Variation with respect to UAV height h_D (a): LoS probability $P^{u^d_i}_{los}$ of different users, (b): NLoS probability $P^{u^d_i}_{nlos}$ of different users, (c): The PL exponent $\alpha^d_{u_i}$ of different users, and (d): PL $PL^{u^d_i}$ encountered by users, incorporating the effects of LoS and NLoS probabilities, PL exponent, LoS and NLoS PL.

of the users served by the UAV as a function of h_D. From Fig. 7(a) and Fig. 7(b), it is observed that $P^{u^d_i}_{los}$ increases and $P^{u^d_i}_{nlos}$ decreases, respectively, with the increase in h_d. The variation of the PL exponent $\alpha_{u^d_i}$ with variation in h_D is illustrated in Fig. 7(c). As indicated by Fig. 7(c), higher UAV altitude results in a smaller value of the PL exponent, owing to the increase in LoS probability with UAV height. Fig. 7(d) illustrates the PL experienced by the users served by the UAV as a function of h_D, incorporating the effects of LoS probability, NLoS probability, PL exponent, and PL due to LoS and NLoS propagation conditions.

UAV-assisted NOMA and OMA data transmission: The simulation parameters used for UAV-assisted NOMA and OMA data transmission are presented in Table III. The target rate of the strongest user, i.e., the user at the least distance from UAV, is considered 1 bit per channel use (BPCU), i.e., $\mathcal{R}_t^{u^d_{N_d}} = 1$ BPCU. For users $u^d_i\, i \neq N_d$, the target rate is considered as $\mathcal{R}_t^{u^d_i} = \beta^d_{u_i} \times \mathcal{R}_t^{u^d_{N_d}}, i \neq N_d$, and $\beta^d_{u_i}$ is given as

$$\beta^d_{u_i} = \frac{r^d_{u_i}}{\sum_{i=1}^{N_d-1} r^d_{u_i}}. \tag{70}$$

For the simulated network scenario, the considered target rates of the users are along the lines of [7]. To solve the proposed optimization frameworks of UAV-assisted NOMA and OMA data transmission utilizing the differential evolution methodology, we consider cross probability, scaling factor, and tolerance for constraint violations as 0.5, 0.6, and 0.001 respectively. The graphs of optimal (minimum) communication power $P^\star_{d,noma}$ and optimal UAV hovering height $h^\star_{D,noma}$ for UAV-assisted NOMA transmission are illustrated in Fig. 8(a) and Fig. 8(b) respectively. From Fig. 8(a) it is observed that as the value of the outage probability threshold ϵ_{th} reduces $P^\star_{d,noma}$ increases owing to the requirement of higher communication power for satisfying the stringent QoS requirements of the users (signified by the smaller values of ϵ_{th}). From Fig. 8(b), it is observed that $h^\star_{D,noma}$ for UAV-assisted NOMA transmission increases with the reduction in ϵ_{th}. This trend of $h^\star_{D,noma}$ is observed as greater UAV height results in better LoS probability, thereby ensuring the stringent QoS requirements of the users associated with the UAV. The trends of the optimal communication power $P^\star_{d,oma}$ and optimal UAV height $h^\star_{d,oma}$ for UAV-assisted OMA data transmission are depicted in Fig. 9(a) and Fig. 9(b) respectively.

TABLE III: SIMULATION PARAMETERS FOR UAV-ASSISTED NOMA AND OMA DATA TRANSMISSION

Parameters	**Values**
Maximum height of building (h_{min})	5 m
Maximum permissible height of UAV (h_{max})	1000 m
Constants $\beta^d_{u_1}$, $\beta^d_{u_2}$, $\beta^d_{u_3}$, $\beta^d_{u_4}$	0.2469, 0.2246, 0.2231, and 0.1777
Power allocation factor $a^d_{u_1}$, $a^d_{u_2}$, $a^d_{u_3}$, $a^d_{u_4}$, and $a^d_{u_5}$	0.2469, 0.2246, 0.2231, 0.1777, and 0.1277

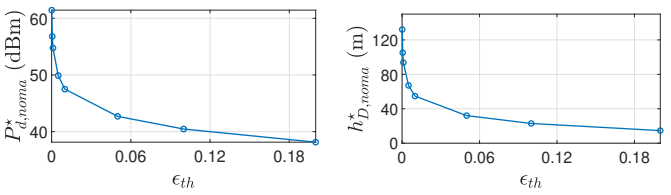

Fig. 8 Variations with outage probability threshold ϵ_{th} for UAV-assisted NOMA transmission (a): Minimum communication power requirement $P^\star_{d,noma}$, (b) optimal UAV hovering height $h^\star_{D,noma}$.

C. Numerical Analysis of Wide Elliptical Beam Design

The convex Hull $\mathcal{H}_d$ formed by the set of users in the UAV set (i.e., the users that are outside the coverage of the gNB)

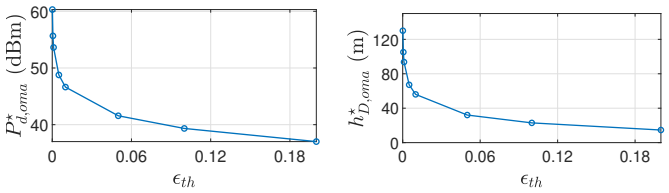

Fig. 9 (a) Minimum communication power requirement $P^{\star}_{d,oma}$ for UAV-assisted OMA transmission for variations in outage probability threshold ϵ_{th}. (b) Optimal UAV hovering height $h^{\star}_{D,oma}$ for OMA transmission for variations in ϵ_{th}.

is depicted in Fig. 10(a). The minimum area ellipse enclosing $\mathcal{H}^d$ is illustrated in Fig. 10(b). Utilizing the parameters of the

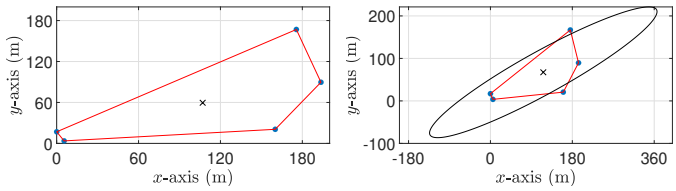

Fig. 10 (a): Convex hull $\mathcal{H}^d$ formed by the users outside the gNB, here, the red polygon represents $\mathcal{H}^d$ and the black cross represents the optimal 2D location of the UAV serving the users outside the gNB. (b): The minimum area ellipse enclosing $\mathcal{H}^d$, herein the black ellipse shows the minimum area ellipse enclosing $\mathcal{H}^d$.

minimum area ellipse formed on the ground plane (Fig. 10(b)), the plots of the designed elliptical beam are illustrated in Fig. 11. The contour plot of the wide elliptical beam at the source plane, i.e., at the UAV is illustrated in Fig. 11(a), while, the 3D gain pattern of the wide elliptical beam is illustrated in Fig. 11(b). The contour plot and 3D gain of the propagated wide elliptical beam on the ground plane are illustrated in Fig. 11(c) and Fig. 11(d), respectively.

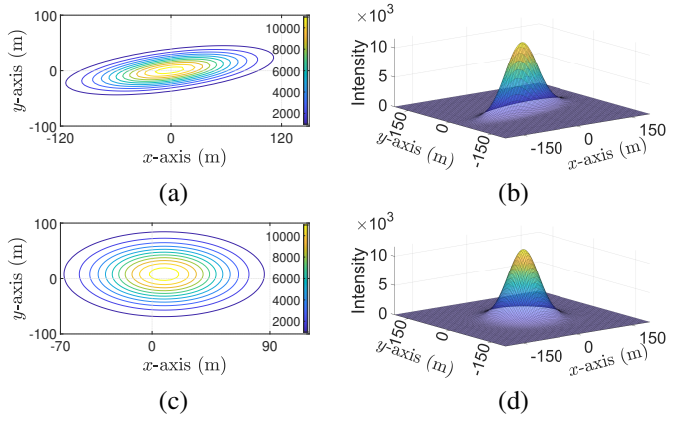

Fig. 11 (a): Contour plot of the 3D pattern of the wide elliptical beam at the source plane, i.e., at the UAV. (b): The 3D gain pattern of the wide elliptical beam at the source plane. (c): Contour plot of wide elliptical beam gain at the destination plane, i.e., the ground plane, wherein the users under the coverage of the UAV are served by the wide elliptical beam. (d): The 3D gain of the designed wide elliptical beam on the ground plane.

D. Numerical Analysis of Dynamic Model and Battery Life of UAV

Dynamic model of UAV: The simulation parameters utilized for the dynamic model of the UAV are listed in Table IV. Fig. 12, illustrates the variations of angular velocity (ω_h), the total current drawn by the rotors, and the total hovering power consumption $\left(P^d_{hov}\right)$ of the UAV for variations in the hovering height (h_D) of the UAV. Fig. 12(a) illustrates the plots of ω_h required for the UAV to hover at different altitudes h_D. As observed from Fig. 12(a), ω_h increase with an increase in h_D. Fig. 12(b) illustrates the total current consumption of the UAV for h_D. The total current consumption increases with the increase in h_D, as ω_h increases with h_D. The variation in P^d_{hov} with h_D is illustrated in Fig. 12(c). As observed from Fig. 12(c), P^d_{hov} increases with an increase in h_D, owing to the increase in ω_h and the corresponding increase in the total current consumption.

TABLE IV: Simulation Parameters for Dynamic Model of UAV

Parameters	**Values**
Average density of air (ρ_0)	$1.2255\,\text{kgm}^{-3}$
Pitch angle of rotor blades (θ_0)	15°
Thrust coefficient (C_t)	0.02
2D lift curve slope (C_{l_α})	5.73
Number of blades (N_b)	6
Cord length (c_l)	0.0157 m
Radius of rotor $\left(R_{r_i} = R_r\right) \forall i = 1, 2, 3, 4$	0.4 m
Rotor solidity $\left(\sigma_r = \frac{N_b c_l}{\pi R_r}\right)$	0.0750
Zero-lift drag coefficient $\left(C_{d_0}\right)$	0.01
Mass of UAV (M_d)	1.3 kg

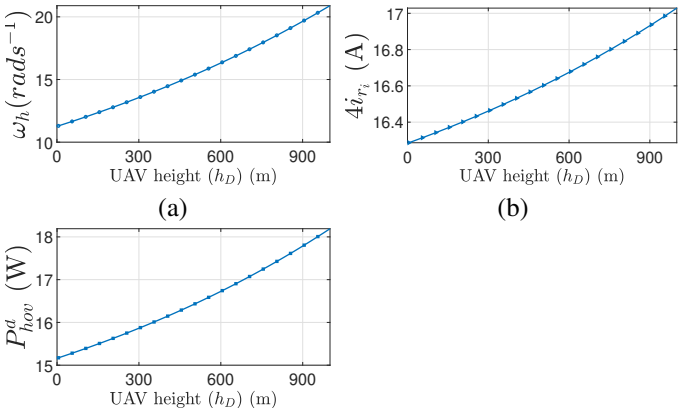

Fig. 12 Variation with respect to UAV hovering height h_D, (a): angular velocity (ω_h) of the rotors of the UAV, (b): total current consumption by the rotors, and (c): hovering power consumption.

Battery life of UAV: The parameters utilized to compute the battery life of the UAV are presented in Table V, here, the parameters pertaining to the battery life of UAV are along the lines of [24]. The proposed graphical methodology to compute the UAV battery life is illustrated in Fig. 13.

TABLE V: Simulation Parameters for Battery Life of UAV

Parameters	**Values**
Resistance $(\mathcal{R})$	0.2Ω
Voltage constant of motor (k_e)	0.0104
Torque constant of motor (k_t)	0.0104
Motor friction torque (T_f)	0.04 Nm
Drag coefficient of motor (k_0)	2.2518×10^{-8}
Motor viscous damping coefficient (D_f)	2×10^{-4} Nmsrad^{-1}
Transceiver voltage of UAV (v_{tr})	1 V
Parameter k_f	4.5×10^{-5}
Splitting factor (μ)	0.9
Battery Capacity (C_{batt})	72000 As

E. Performance Evaluation of the Proposed Framework

The comparison of optimal (minimum) communication power requirements $P^{\star}_{d,noma}$ using our proposed framework

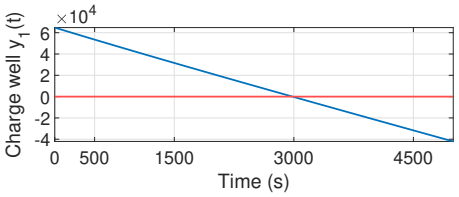

Fig. 13 Proposed graphical methodology to compute the UAV battery life, herein, the intersection of the blue and red line gives the battery life.

of UAV-assisted NOMA data transmission coupled with the generation of a wide elliptical beam is illustrated in the bar graphs of Fig. 14(a). From Fig. 14(a), it is observed that the desired QoS of the users is met with lesser communication power using the proposed framework, thereby resulting in enhanced battery life of the UAV. The comparison between the proposed methodology in terms of the optimal UAV hovering height $h^{\star}_{D,noma}$ required to meet the desired QoS of ground users is illustrated in Fig. 14(b). It is observed from Fig. 14(b), that the desired QoS requirements of the ground users are met at smaller values of $h^{\star}_{D,noma}$ using our proposed approach, here, the smaller value of $h^{\star}_{D,noma}$ results in lower PL, thereby resulting in less communication power consumption and an enhanced battery life of the UAV. The comparison between the proposed methodology and the NOMA-assisted data transmission in terms of the angular velocity ω_h of the rotors of the UAV and the total current consumption by the rotors of the UAV at the optimal UAV hovering height is illustrated in Fig. 15(a) and Fig. 15(b), respectively. Fig. 15(a) and Fig. 15(b) illustrate that by utilizing the proposed methodology, marginally less ω_h is obtained at $h^{\star}_{D,noma}$, thereby resulting in lower total current consumption by the rotors. The performance comparison of the proposed

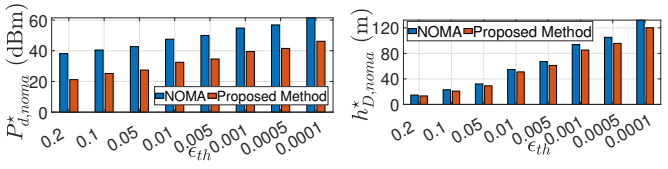

Fig. 14 Comparison of the proposed UAV-assisted NOMA transmission in terms of (a): optimal communication power and (b): optimal UAV hovering height.

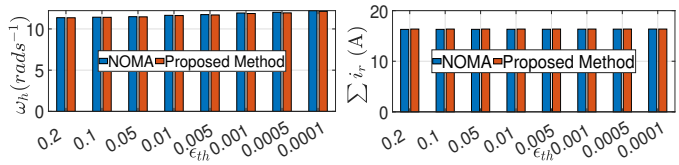

(a) (b)

Fig. 15 Comparison of the proposed UAV-assisted NOMA framework in terms of (a): angular velocity of the rotors and (b): total current consumption by the rotors of the UAV.

methodology in terms of the total hovering power consumption P^{d}_{hov} by the UAV and the battery life of the UAV is illustrated in Fig. 16(a) and Fig. 16(b), respectively. Fig. 16(a) shows that utilization of the proposed methodology results in marginally lower P^{d}_{hov}. Fig. 16(b) illustrates that the proposed methodology significantly enhances the battery life of the UAV owing to the reduction of communication power, UAV hovering height, angular velocity, and current consumption by the UAV. The comparison of minimum communication power

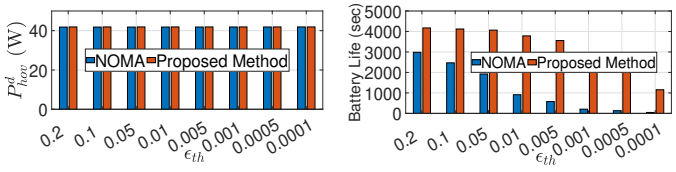

(a) (b)

Fig. 16 Comparision of the proposed UAV-assisted NOMA transmission in terms of (a): hovering power consumption, (b): UAV battery life.

requirements using our proposed framework of UAV-assisted OMA transmission is illustrated in the bar graphs of Fig. 17(a). From Fig. 17(a), it is observed that the desired QoS of the users is met with lesser communication power using the proposed method. The comparison between the proposed

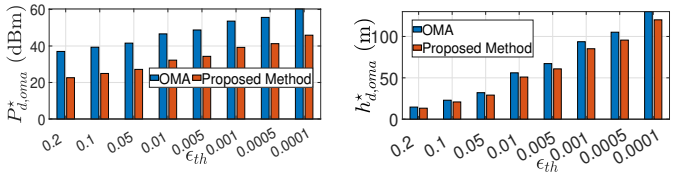

(a) (b)

Fig. 17 (a): Comparison of the proposed UAV-assisted OMA transmission framework in terms of (a): optimal communication and (b): optimal UAV hovering height.

methodology and the OMA-assisted data transmission in terms of the optimal UAV hovering height is illustrated in Fig. 17(b). From Fig. 17(b), it is observed that the ground users' desired QoS requirements are met at lower UAV heights using our proposed approach. The comparison between the proposed methodology and the OMA-assisted data transmission scheme in terms of the angular velocity of the rotors of the UAV and the total current consumption by the rotors of the UAV at the computed optimal UAV hovering height is illustrated in Fig. 18(a) and Fig. 18(b), respectively. The performance

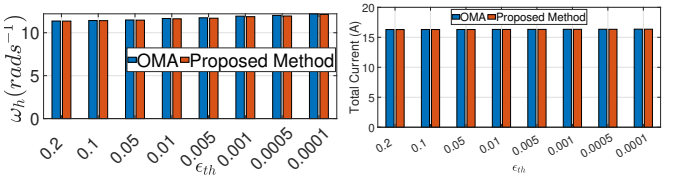

(a) (b)

Fig. 18 Comparison of the proposed UAV-assisted OMA transmission framework in terms of (a): angular velocity of the rotors and (b): total current consumption by the rotors of the UAV.

comparison of the proposed methodology in terms of the total hovering power consumption by the UAV for OMA-assisted transmission and the total battery life of the UAV for OMA-assisted transmission is illustrated in Fig. 19(a) and Fig. 19(b), respectively, herein, a significantly longer UAV battery life is achieved for UAV-assisted OMA transmission utilizing the proposed framework.

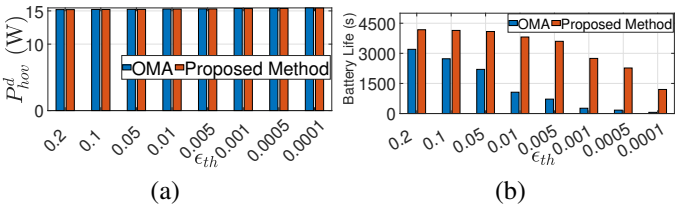

(a) (b)

Fig. 19 Comparison of the proposed UAV-assisted OMA transmission in terms of (a): hovering power consumption of UAV and (b) UAV battery life.

X. Conclusions

In this paper, we presented a joint framework incorporating gNB and UAV-assisted NOMA and OMA data transmission schemes to serve the spatially separated users in a given rural geographical area of interest, wherein the users outside the gNB are served by the UAV. In this regard, we first presented an optimization framework to compute the optimum coverage radius of the gNB constrained by the coverage probability utilizing the RMa prorogation scenario. Thereafter, we presented optimization frameworks to compute the minimum communication power and optimal UAV hovering height to meet the desired QoS of the users characterized by outage probability for UAV-assisted NOMA and OMA transmission. Going, further, we studied wide elliptical beam design to serve the users under the coverage of UAV and further, we analyzed the angular velocity of rotors, the total current consumption by the rotors, and the hovering power consumption of the UAV. Furthermore, we proposed a graphical methodology to determine the battery life of a LiPo battery-powered UAV. The performance evaluation demonstrated the superior performance of the proposed framework in communication power requirement and battery life of UAV compared to the conventional UAV-assisted NOMA and OMA transmission.

References

[1] Y. Qin, M. A. Kishk, and M.-S. Alouini, "Drone charging stations deployment in rural areas for better wireless coverage: Challenges and solutions," *IEEE IoT Mag.*, vol. 5, no. 1, pp. 148–153, 2022.

[2] R. De Gaudenzi, M. Luise, and L. Sanguinetti, "The open challenge of integrating satellites into (beyond-) 5G cellular networks," *IEEE Network*, vol. 36, no. 2, pp. 168–174, 2022.

[3] M. Matracia, M. A. Kishk, and M.-S. Alouini, "Coverage analysis for UAV-assisted cellular networks in rural areas," *IEEE Open J. Veh. Technol.*, vol. 2, pp. 194–206, 2021.

[4] G. Airlangga and A. Liu, "Online path planning framework for UAV in rural areas," *IEEE Access*, vol. 10, pp. 37572–37585, 2022.

[5] M. Gharib, S. Nandadapu, and F. Afghah, "An exhaustive study of using commercial LTE network for UAV communication in rural areas," in *2021 IEEE ICC Workshops*, pp. 1–6, 2021.

[6] Y. Liu, Z. Qin, Y. Cai, Y. Gao, G. Y. Li, and A. Nallanathan, "UAV communications based on non-orthogonal multiple access," *IEEE Wireless Commun.*, vol. 26, no. 1, pp. 52–57, 2019.

[7] D.-T. Do, A.-T. Le, Y. Liu, and A. Jamalipour, "User grouping and energy harvesting in UAV-NOMA system with AF/DF relaying," *IEEE Trans. Veh. Technol.*, vol. 70, no. 11, pp. 11855–11868, 2021.

[8] S. Fu, X. Guo, F. Fang, Z. Ding, N. Zhang, and N. Wang, "Towards energy-efficient data collection by unmanned aerial vehicle base station with NOMA for emergency communications in IoT," *IEEE Trans. Veh. Technol.*, vol. 72, no. 1, pp. 1211–1223, 2023.

[9] D. Zhai, H. Li, X. Tang, R. Zhang, Z. Ding, and F. R. Yu, "Height optimization and resource allocation for NOMA enhanced UAV-aided relay networks," *IEEE Trans. Commun.*, vol. 69, no. 2, pp. 962–975, 2021.

[10] X. Mu, Y. Liu, L. Guo, J. Lin, and Z. Ding, "Energy-constrained UAV data collection systems: NOMA and OMA," *IEEE Trans. Veh. Technol.*, vol. 70, no. 7, pp. 6898–6912, 2021.

[11] 3GPP, "Technical Specification Group Radio Access Network;Study on channel model for frequency spectrum above 6 GHz (Rel. 15)." TR 38.900 V15.0.0, 2018.

[12] S. Takenaga, Y. Ozaki, and M. Onishi, "Practical initialization of the nelder–mead method for computationally expensive optimization problems," *Optimization Lett.*, vol. 17, no. 2, pp. 283–297, 2023.

[13] M. M. Azari, F. Rosas, K.-C. Chen, and S. Pollin, "Ultra reliable UAV communication using altitude and cooperation diversity," *IEEE Trans. Commun.*, vol. 66, no. 1, pp. 330–344, 2018.

[14] Y. Liu, K. Xiong, Y. Lu, Q. Ni, P. Fan, and K. B. Letaief, "UAV-aided wireless power transfer and data collection in Rician fading," *IEEE J. Sel. Areas Commun.*, vol. 39, no. 10, pp. 3097–3113, 2021.

[15] A. Al-Hourani, S. Kandeepan, and S. Lardner, "Optimal LAP altitude for maximum coverage," *IEEE Wireless Commun. Lett.*, vol. 3, no. 6, pp. 569–572, 2014.

[16] B. Makki, K. Chitti, A. Behravan, and M.-S. Alouini, "A survey of NOMA: Current status and open research challenges," *IEEE Open J. Commun. Soc.*, vol. 1, pp. 179–189, 2020.

[17] W. Deng, S. Shang, X. Cai, H. Zhao, Y. Song, and J. Xu, "An improved differential evolution algorithm and its application in optimization problem," *Soft Computing*, vol. 25, pp. 5277–5298, 2021.

[18] Z. Wu, S. Jiang, X. Zhou, Y. Wang, Y. Zuo, Z. Wu, L. Liang, and Q. Liu, "Application of image retrieval based on convolutional neural networks and hu invariant moment algorithm in computer telecommunications," *Computer Commun.*, vol. 150, pp. 729–738, 2020.

[19] A. A. Kovalev, V. V. Kotlyar, and D. S. Kalinkina, "Propagation-invariant off-axis elliptic gaussian beams with the orbital angular momentum," in *Photonics*, vol. 8, p. 190, MDPI, 2021.

[20] M. Mozaffari, W. Saad, M. Bennis, and M. Debbah, "Communications and control for wireless drone-based antenna array," *IEEE Trans. Commun.*, vol. 67, no. 1, pp. 820–834, 2018.

[21] U. Demir, M. İpek, C. Toker, and Ekici, "Energy-efficient rotary-wing UAV deployment under flight dynamics and QoS constraints," in *2019 IEEE BlackSeaCom*, pp. 1–5, 2019.

[22] V. M. Arellano-Quintana, E. A. Merchán-Cruz, and A. Franchi, "A novel experimental model and a drag-optimal allocation method for variable-pitch propellers in multirotors," *IEEE Access*, vol. 6, pp. 68155–68168, 2018.

[23] F. Morbidi, R. Cano, and D. Lara, "Minimum-energy path generation for a quadrotor UAV," in *2016 IEEE ICRA*, pp. 1492–1498, IEEE, 2016.

[24] W. Jaafar and H. Yanikomeroglu, "Dynamics of laser-charged UAVs: A battery perspective," *IEEE IoT J.*, vol. 8, no. 13, pp. 10573–10582, 2020.

[25] I. Azam, M. B. Shahab, and S. Y. Shin, "Energy-efficient pairing and power allocation for NOMA UAV network under QoS constraints," *IEEE Internet of Things J.*, vol. 9, no. 24, pp. 25011–25026, 2022.

[26] P. K. Sharma and D. I. Kim, "Random 3D mobile UAV networks: Mobility modeling and coverage probability," *IEEE Trans. Wireless Commun.*, vol. 18, no. 5, pp. 2527–2538, 2019.

[27] J. Lorincz, Z. Klarin, and D. Begusic, "Modeling and analysis of data and coverage energy efficiency for different demographic areas in 5G networks," *IEEE Syst. J.*, vol. 16, no. 1, pp. 1056–1067, 2022.

[28] T. Bose, A. Suresh, O. J. Pandey, L. R. Cenkeramaddi, and R. M. Hegde, "Improving quality-of-service in cluster-based UAV-assisted edge networks," *IEEE Trans. Network and Service Manage.*, vol. 19, no. 2, pp. 1903–1919, 2022.